

Electronic Supporting Information (ESI):

Unprecedented Hexagonal Bipyramidal Single-Ion Magnets Based on Metallacrowns

Quan-Wen Li,^a Rui-Chen Wan,^a Yan-Cong Chen,^a Jun-Liang Liu,^a Long-Fei Wang,^a Jian-Hua Jia,*^a Nicholas F. Chilton^b and Ming-Liang Tong*^a

^a MOE Key Lab of Bioinorganic and Synthetic Chemistry, School of Chemistry, Sun Yat-Sen University, Guangzhou 510275, P. R. China

^b School of Chemistry, The University of Manchester, Oxford Road, Manchester M13 9PL, U.K.
E-mail: jiajh3@mail.sysu.edu.cn; tongml@mail.sysu.edu.cn.

CONTENTS

- Page 2** **Experimental Section** Materials and physical measurements, single crystal X-ray crystallography, synthesis and CASSCF-SO calculations.
- Page 3** **Fig. S1.** Experimental and simulated X-ray powder diffraction (XRPD) patterns for **1** and **2**.
Fig. S2. Thermogravimetric analysis of **1** and **2**.
- Page 4** **Table S1.** Crystallographic Data and Structural Refinements for **1** and **2**.
Fig.S3. Outer coordination sphere of **1** and **2**.
- Page 5** **Table S2.** Selected bonds lengths and angles for **1** and **2**.
Table S3. Comparison of equatorial coordination environment in **1**, **2** and some other reported equatorial 6-coordination systems.
- Page 6** **Table S4.** Lanthanide ion geometry analysis by using SHAPE 2.0 program.
Table S5. Comparison of axial Ce(Nd)-O_{po} distances and O_{po}-Ce(Nd)-O_{po} angles in **1**, **2** and some other cases.
Table S6. Cd(II) ion geometry analysis by using SHAPE 2.0 program.
- Page 7** **Fig.S4.** Plots of *M*-*H/T* at 2.0, 3.0, and 5.0 K for **1** and **2**.
Table S7 Energy levels and eigenstates for compounds **1** and **2**.
Fig. S5. The field-dependent of the relaxation time for **1** and **2** at 1.8K.
- Page 8** **Table S8.** The fitting parameters of field-dependent relaxation data for **1** and **2**.
Fig S6. Temperature dependence of the in-phase $\chi'_m T$ and out-of-phase χ''_m for **1** and **2**.
- Page 9** **Fig. S7.** Cole–Cole plots for the ac susceptibilities of **1** and **2**.
Table S9. Comparison of **1** and **2** with reported Ce(III) and Nd(III) SIMs.
- Page 10** **Fig. S8.** The temperature-dependent relaxation time for **1** and **2**.
Table S10. The fitting parameters of temperature-dependent relaxation data.
- Page11** **References**

EXPERIMENTAL SECTION

Materials and Physical Measurements. The ligand H₂quinHA was synthesized as literature described¹. Metal salts and other reagents were commercially available and used as received without further purification. The C, H, and N elemental analyses were carried out with an Elementar Vario-EL CHNS elemental analyzer. X-ray powder diffraction (XRPD) performed on polycrystalline samples were measured at 293 K on Bruker D8 Advance Diffratometer (Cu- K_{α} , $\lambda = 1.54056 \text{ \AA}$) by scanning over the range of 5-50° with step of 0.2/s. Simulated patterns were generated with Mercury. Magnetic susceptibility measurements were performed with a Quantum Design MPMS-XL7 SQUID. Polycrystalline samples were embedded in vaseline to prevent torqueing. Data were corrected for the diamagnetic contribution calculated from Pascal constants.

Single Crystal X-ray Crystallography. Diffraction data were collected on a Bruker APEXIII CCDIII diffractometer with Mo K α radiation ($\lambda = 0.71073 \text{ \AA}$) for complexes **1** and **2** at 120(2) K. The Data indexing and integration were carried out using a Bruker Smart program. The structures were solved by direct methods, and all non-hydrogen atoms were refined anisotropically by least-squares on F^2 using the SHELXTL 2014 program suite². Anisotropic thermal parameters were assigned to all non-hydrogen atoms. The hydrogen atoms attached to carbon, nitrogen and oxygen atoms were placed in idealised positions and refined using a riding model to the atom to which they were attached. The disordered solvent molecules were squeezed³ and determined by the elemental analysis and thermogravimetric analysis. CCDC 1498048 (**1**) and 1498049 (**2**) contain the supplementary crystallographic data for this paper. These data can be obtained free of charge via www.ccdc.cam.ac.uk/conts/retrieving.html (or from the Cambridge Crystallographic Data Centre, 12 Union Road, Cambridge CB21EZ, UK; fax: (+44)1223-336-033; or deposit@ccdc.cam.ac.uk).

Synthesis. [CeCd₃(Hquinha)₃(n-Bu₃PO)₂I₃]3EtOH·2H₂O (**1**): A mixture of H₂quinHA (0.075 mmol, 14.1 mg) and CdI₂ (0.075 mmol, 27.5 mg) was dissolved in 5 mL EtOH. Under stirring, Ce(NO₃)₃·6H₂O (0.025 mmol, 10.9 mg) and tributylphosphine oxide (0.05 mmol, 10.9 mg) were added to the solution successively. The solution was kept stirring for a minute and then filter before becoming heavy cloudy. Colourless crystals suitable for X-ray analysis were obtained in several days by slow evaporation. Yield: 49.8%. Elemental analysis calcd (%) for CeCd₃I₆P₂C₆₀H₉₇N₆O₁₃; C: 29.89, H: 4.05, N: 3.49; found (%): C: 29.66, H: 3.82, N: 3.52.

[NdCd₃(Hquinha)₃(n-Bu₃PO)₂I₃]3EtOH·2H₂O (**2**): the procedure was the same as that employed for complex **1**, except that Ce(NO₃)₃·6H₂O was replaced by Nd(NO₃)₃·6H₂O (0.025 mol, 11.0 mg). Colourless crystals were obtained in several days by slow evaporation. Yield: 42.2%. Elemental analysis calcd (%) for NdCd₃I₆P₂C₆₀H₉₇N₆O₁₃; C: 29.84, H: 4.05, N: 3.48; found (%): C: 29.93, H: 3.92, N: 3.24.

CASSCF-SO calculations. The X-ray structures of **1** and **2** were used without optimisation. Basis sets from the ANO-RCC library were employed, with VTZP quality for the Ln atoms, VDZP quality for the first coordination sphere atoms, and VDZ quality for all other atoms. The two electron integrals were Cholesky decomposed with a threshold of 1×10^{-8} . The state-averaged CASSCF calculations were performed using 1 electron in 7 orbitals with 7 doublets for **1**, and 3 electrons in 7 orbitals with 35 quartets and 112 doublets for **2**. All roots were included in the spin orbit mixing for both complexes. The CF decomposition of the ground $J = 5/2$ and $J = 9/2$ multiplets for **1** and **2**, respectively, were performed with the SINGLE_ANISO module.

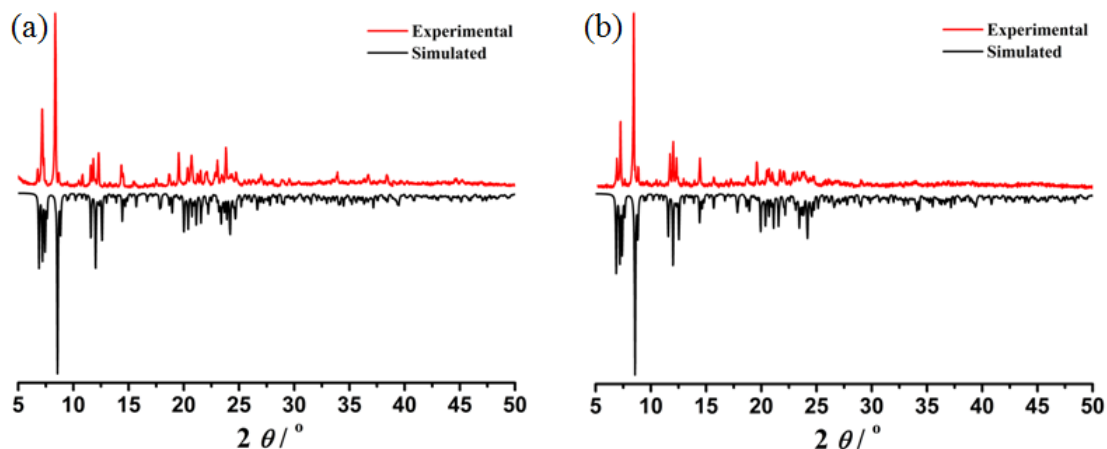


Fig. S1. Experimental and simulated X-ray powder diffraction (XRPD) patterns for **1** (a) and **2** (b).

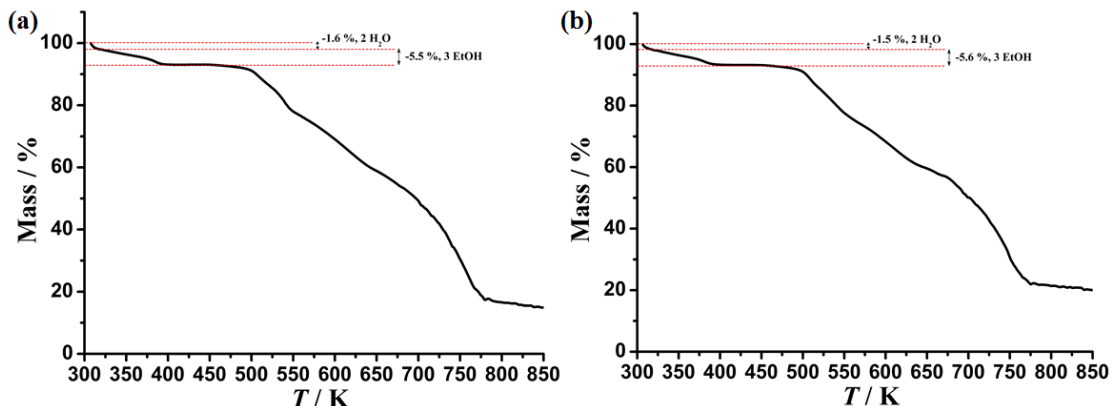


Fig. S2. Thermogravimetric analysis of **1** (a) and **2** (b). The red dash lines show the two stages of escaping of solvent molecules. When the temperature increases, the two disordered H_2O molecules escape first. Then, the three ethanol molecules connected to the $\{\text{LnCd}_3\}$ core with $\text{O}-\text{H}\cdots\text{I}$ weak interactions escape in higher temperatures.

Table S1. Crystallographic Data and Structural Refinements for **1** and **2**.

Compound	1	2
Formula	CeCd ₃ I ₆ P ₂ C ₆₀ H ₉₃ N ₆ O ₁₁	NdCd ₃ I ₆ P ₂ C ₆₀ H ₉₃ N ₆ O ₁₁
Formula weight	2375.06	2379.18
Temperature / K	120(2)	120(2)
Crystal system	Monoclinic	Monoclinic
Space group	<i>P</i> 2 ₁ /c	<i>P</i> 2 ₁ /c
<i>a</i> / Å	26.1665(13)	26.2751(9)
<i>b</i> / Å	15.2608(8)	15.2788(6)
<i>c</i> / Å	23.2073(10)	23.1448(7)
β / °	114.863(1)	114.769(1)
<i>V</i> / Å ³	8408.3(7)	8436.7(5)
<i>Z</i>	4	4
$\rho_{calcd.}$ (g/cm ³)	1.876	1.873
μ (mm ⁻¹)	3.571	3.635
<i>F</i> (000)	4532	4540
Reflections collected	59415	61138
Independent reflections	19263	19369
GOF on <i>F</i> ²	1.053	1.013
<i>R</i> ₁ , <i>wR</i> ₂ [<i>I</i> ≥ 2σ(<i>I</i>)] ^a	0.0626, 0.1298	0.0415, 0.0745
<i>R</i> ₁ , <i>wR</i> ₂ (all data) ^b	0.1048, 0.1449	0.0732, 0.0834
CCDC No.	1498048	1498049

^a $R_1 = \sum |Fo| - |Fc| / \sum |Fo|$. ^b $wR_2 = [\sum w(Fo^2 - Fc^2)^2 / \sum w(Fo^2)]^{1/2}$.

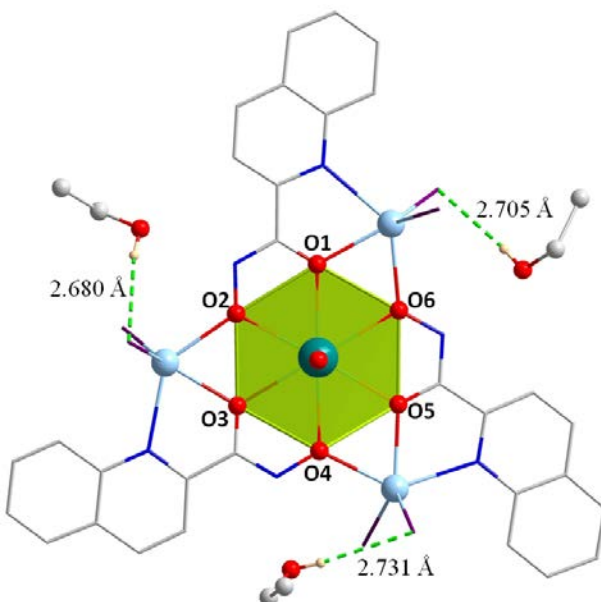


Fig.S3. Outer coordination sphere, connected with O–H···I weak interactions (green dash lines) of **1** and **2**. H atoms of the ligands are omitted for clarity. The colours of teal, pale blue, violet, pink, blue, red and light grey represent for Ln, Cd, I, P, N, O and C atoms, respectively. The green hexagonal area shows the planar coordination environment of Ln ion.

Table S2. Selected bonds lengths [Å] and angles [°] for **1** and **2**.*

	1		2
Ce1-O1	2.531(5)	Nd1-O1	2.508(3)
Ce1-O2	2.516(6)	Nd1-O2	2.483(3)
Ce1-O3	2.535(5)	Nd1-O3	2.508(3)
Ce1-O4	2.532(6)	Nd1-O4	2.511(4)
Ce1-O5	2.514(5)	Nd1-O5	2.488(3)
Ce1-O6	2.537(6)	Nd1-O6	2.526(3)
Ce1-O7	2.356(6)	Nd1-O7	2.312(4)
Ce1-O8	2.317(6)	Nd1-O8	2.290(4)
O1-Ce1-O2	61.00(18)	O1-Nd1-O2	61.57(11)
O2-Ce1-O3	59.62(17)	O2-Nd1-O3	59.80(11)
O3-Ce1-O4	60.78(18)	O3-Nd1-O4	61.26(11)
O4-Ce1-O5	59.91(18)	O4-Nd1-O5	59.95(11)
O5-Ce1-O6	60.53(17)	O5-Nd1-O6	60.73(11)
O6-Ce1-O1	60.17(17)	O6-Nd1-O1	59.77(11)
O7-Ce1-O8	178.3(3)	O7-Nd1-O8	179.00(14)

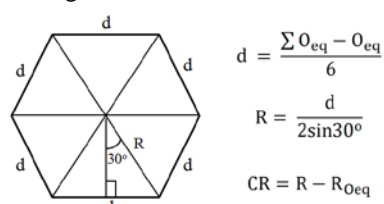
* The atoms are labelled as shown in Fig. S3 and the text.

Table S3. Comparison of equatorial coordination environment in **1**, **2** and some other reported equatorial 6-coordination systems.

Compounds*	Ce(Nd)-O _{eq} distances (Å)	Cavity radius (Å)**	Range of θ angles	Ref
1	2.514–2.537	1.24	59.63–61.00	This work
[Cu ₃ Ce(L ¹)(NO ₃) ₃ (MeOH) ₃]	2.487–2.621	1.26	57.42–62.03	4
[Ce(18-C-6)(L ²) ₂][Ce(L ²) ₄]	2.582–2.637	1.33	59.15–62.09	5
[Ce(18-C-6)(BH ₄) ₂](BPh ₄)	2.617–2.660	1.34	59.81–61.14	6
[Ce(18-C-6)(H ₂ O)Cl ₂]Cl·2H ₂ O	2.576–2.641	1.39	60.34–62.85	7
2	2.483–2.527	1.22	59.77–61.57	This work
[Nd(18-C-6)(BH ₄) ₂](BPh ₄)	2.624–2.671	1.34	59.36–60.45	6
[NdB ₃ (L ³) ₆ (C ₄ H ₈ O) ₃]·C ₄ H ₈ O	2.406–2.430	1.09	54.05–64.51	8
[Nd(18-C-6)(H ₂ O) ₂ Cl]Cl ₂ ·2H ₂ O	2.541–2.608	1.37	60.96–64.15	9

*O_{eq} stands for equatorial coordinated oxygen atoms. L¹ = [3+3] macrocyclic ligands; L² = N(SiMe₃)Ph^F, Ph^F = pentafluorophenyl; L³ = η²-catechol-μ-catecholborate.

**The cavity radius is calculated according to a literature¹⁰. The method can be described as:



CR = Cavity Radius; R_{Oeq} means the radius of O_{eq} atoms on the ring with an estimated value of 1.30 Å. See details in the literature¹⁰.

Table S4. Lanthanide geometry analysis by using SHAPE 2.0 program.*

	HBPY(D_{6h})	CU(O_h)	SAPR(D_{4d})	TDD(D_{2d})
Ce1	0.456	6.862	15.417	12.931
Nd1	0.644	6.600	14.634	12.157

*HBPY = Hexagonal bipyramid; Cu = Cube; SAPR = Square antiprism; TDD = Triangular dodecahedron.

Table S5. Comparison of axial Ce(Nd)-O_{po} distances and O_{po}-Ce(Nd)-O_{po} angles in **1**, **2** and some other cases.

Compounds*	Ce(Nd)-O _{po} distances (Å)	O _{po} -Ce(Nd)-O _{po} angle (°)	Ref
1	2.317, 2.356	178.3	This work
[Ce(L ⁴) ₂ (H ₂ O) ₂ Cl ₃]	2.371	169.9	11
2	2.290, 2.312	179.0	This work
[Nd(L ⁵)(H ₂ O) ₅]I ₃ ·(L ⁵) ₂ ·H ₂ O	2.285, 2.294	174.4	12
[Nd(L ⁶) ₂ (NO ₃) ₃ (H ₂ O)]·2EtOH	2.345, 2.369	151.7	13
[Nd(L ⁷) ₂ (NO ₃) ₃ (H ₂ O)]	2.349, 2.353	148.66	14

*L⁴ = *P,P*-dimorpholino-N-phenylphosphinic amide; L⁵ = ^tBu (NH^tPr)₂PO; L⁶ = (^tBu)3PO; L⁷ = 2-(2-(dio-tolylphosphoryl)ethyl)benzo[d]oxazole;

Table S6. Cd(II) ion geometry analysis by using SHAPE 2.0 program and the parameter τ of deviation from trigonal bipyramidal and square pyramid.*

	PP	VOC	TBPY	SPY	JTBPY	τ
Cd1 in 1	33.515	10.053	5.334	6.204	10.421	0.22
Cd2 in 1	35.413	10.100	5.098	5.963	10.333	0.23
Cd3 in 1	32.424	10.463	5.352	6.497	10.738	0.24
Cd1 in 2	33.017	10.159	5.516	6.276	10.643	0.21
Cd2 in 2	34.934	10.077	5.240	5.921	10.598	0.23
Cd3 in 2	32.273	10.797	5.486	6.684	10.958	0.23

*PP = Pentagon; VOC = Vacant octahedron; TBPY = Trigonal bipyramidal; SPY = Spherical square pyramid; JTBPY = Johnson Trigonal.

The parameter τ is calculated according to the literature.¹⁵

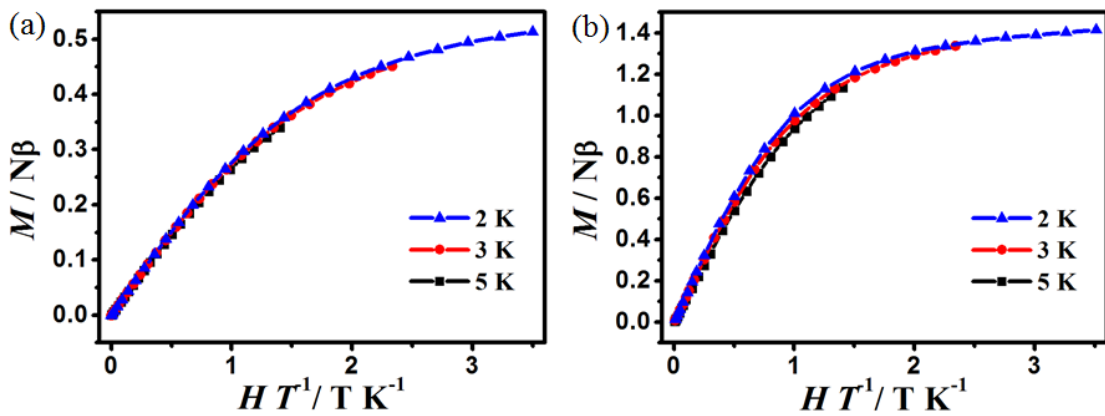


Fig.S4. Plots of $M-H/T$ at 2.0, 3.0, and 5.0 K for **1** (a) and **2** (b). The solid line is a guide for the eyes.

Table S7. Energy levels and eigenstates for compounds **1** and **2** calculated with CASSCF-SO. Wavefunctions decomposed along the pseudo- D_6 axis.

	Energy / cm ⁻¹	g_x	g_y	g_z	Angle / °	Crystal field wavefunctions $ m_J\rangle$
1	0	0.02	0.10	2.48	-	96% $ \pm 3/2\rangle$
	303	0.22	0.27	3.82	23	97% $ \pm 5/2\rangle$
	784	0.60	2.46	2.58	83	81% $ \pm 1/2\rangle$ + 19% $ \mp 1/2\rangle$
2	0	0.07	0.21	4.18	-	71% $ \pm 9/2\rangle$ + 29% $ \mp 3/2\rangle$
	104	0.36	2.49	2.66	87	39% $ \pm 5/2\rangle$ + 25% $ \mp 5/2\rangle$ + 20% $ \mp 7/2\rangle$ + 15% $ \pm 7/2\rangle$
	215	0.55	2.72	4.08	87	76% $ \pm 1/2\rangle$ + 17% $ \mp 1/2\rangle$
	289	0.25	0.89	1.67	81	67% $ \pm 3/2\rangle$ + 27% $ \mp 9/2\rangle$
	586	1.80	2.85	2.96	83	62% $ \pm 7/2\rangle$ + 36% $ \mp 5/2\rangle$

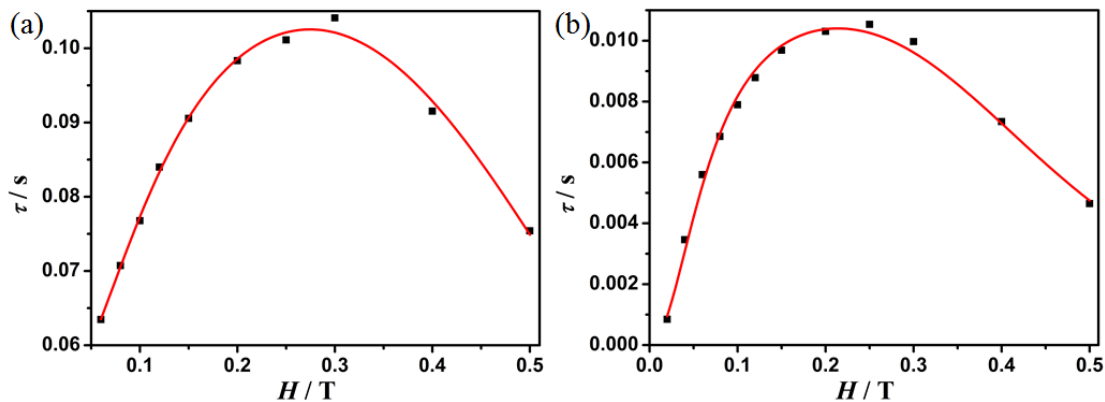


Fig.S5. The field-dependent relaxation time for **1** (a) and **2** (b) at 1.8K. The red lines are the fitness with equation (2) in the text.

Table S8. The fitting parameters of field-dependent relaxation data with the direct, QTM and field-independent processes for **1(a)** and **2(b)**.

	A ($\text{s}^{-1} \text{Oe}^{-4} \text{K}^{-1}$)	B_1 (s^{-1})	B_2 (Oe^{-2})	$D(\text{s}^{-1})$
1	4.13E-15	11.29	1.50E-6	8.42
2	1.08E-13	5330.37	1.36E-4	83.40

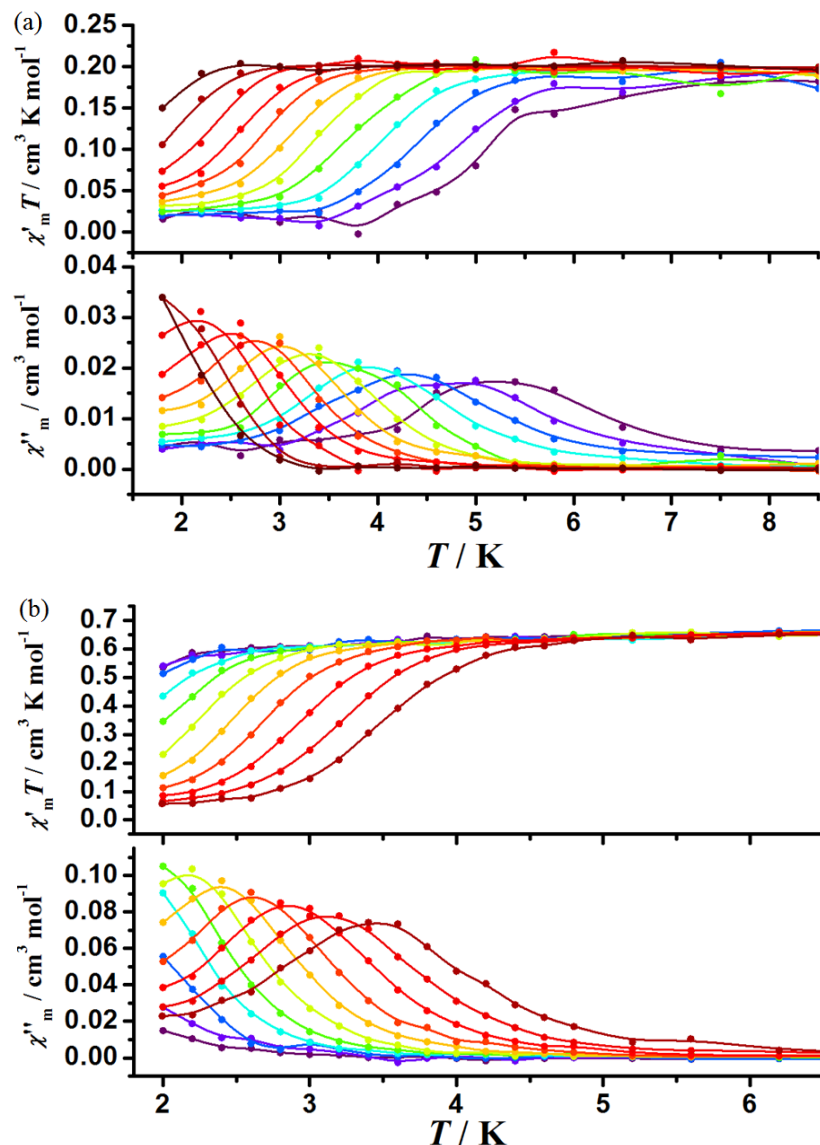


Fig.S6. Temperature dependence of the in-phase $\chi'_m T$ product and out-of-phase χ''_m in a 1500 Oe dc field for **1** (a) and a 2500 Oe dc field for **2** (b). The solid lines are guides for the eyes.

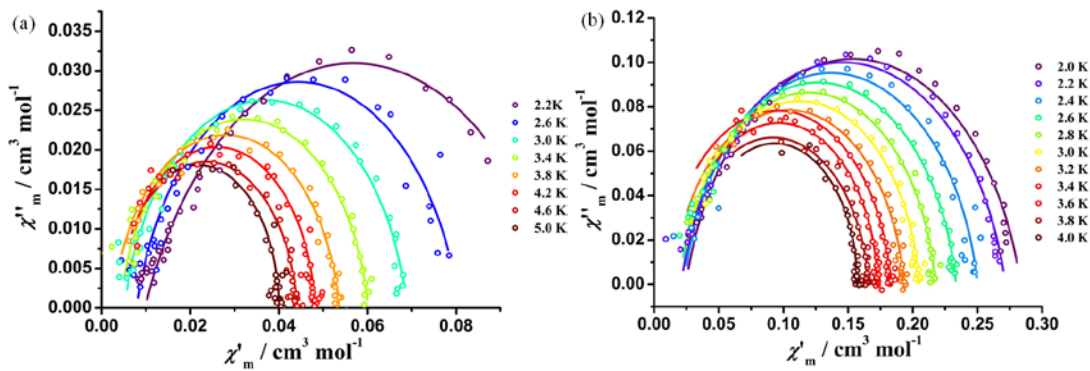


Fig.S7.Cole–Cole plots for the ac susceptibilities in a 1500 Oe dc field for **1** (a) and a 2500 Oe dc field for **2** (b). The solid lines are the best fit to the generalized Debye model.

Table S9.Comparison of **1** and **2** with reported Ce(III) and Nd(III) SIMs.

Compounds*	$U_{\text{eff}} / \text{K}$	τ_0 / s	Ref
1	27	8.2×10^{-7}	This work
[CeZn ₂ (L ⁸) ₂ I ₂ (MeOH)]BPh ₄	21.2	1.6×10^{-7}	16
[CeZn ₂ (L ⁹) ₂ (AcO) ₂]BPh ₄	37	2.7×10^{-7}	17
Li(DME) ₃ [Ce(COT'') ₂]	30	1.2×10^{-6}	18
[Ce(dmso) ₈][Ce(η^2 -NO ₃) ₂ (dmso) ₄ (α -Mo ₈ O ₂₆) _{0.5}][Mo ₆ O ₁₉]	24.4 4.4 9.1	2.56×10^{-7} 2.09×10^{-5} 1.12×10^{-6}	19
[Ce(NO ₃) ₂ {Zn(L ⁹)(SCN)} ₂]·CH ₃ CN	35.7	2.2×10^{-7}	20
2	22	3.9×10^{-7}	This work
[Nd(NO ₃) ₂ {Zn(L ⁹)(SCN)} ₂]·CH ₃ CN	38.5	2.07×10^{-7}	20
NdT ₃	4.08	1.2×10^{-5}	21
{[Ln ₂ (CNCH ₂ COO) ₆ (H ₂ O) ₄] ₂ H ₂ O} _n	26.6	1.75×10^{-7}	22
Na ₉ [Nd(W ₅ O ₁₈) ₂] ₃ ·2H ₂ O	74	3.55×10^{-10}	23
[Li(DME) ₃][Nd(COT'') ₂]	21	5.5×10^{-5}	24
[Nd(L ⁵)(H ₂ O) ₅]I ₃ ·(L ⁵) ₂ ·H ₂ O	39.21	8.98×10^{-7}	12

*L⁸ = 6,6'-(1E,1'E)-(2,2-dimethylpropane-1,3-diyl)bis(azan-1-yl-1-ylidene)bis(methan-1-yl-1-ylidene)

bis(2-methoxyphenol) ;

L⁹ = 6,6'-(1E,1'E)-(ethane-1,2-diylbis(azan-1-yl-1-ylidene))bis(methan-1-yl-1-ylidene)bis(2-methoxy phenol);

COT'' = bis(trimethylsilyl)cyclooctatetraenyl dianion;

Tp⁻ = trispyrazolylborate.

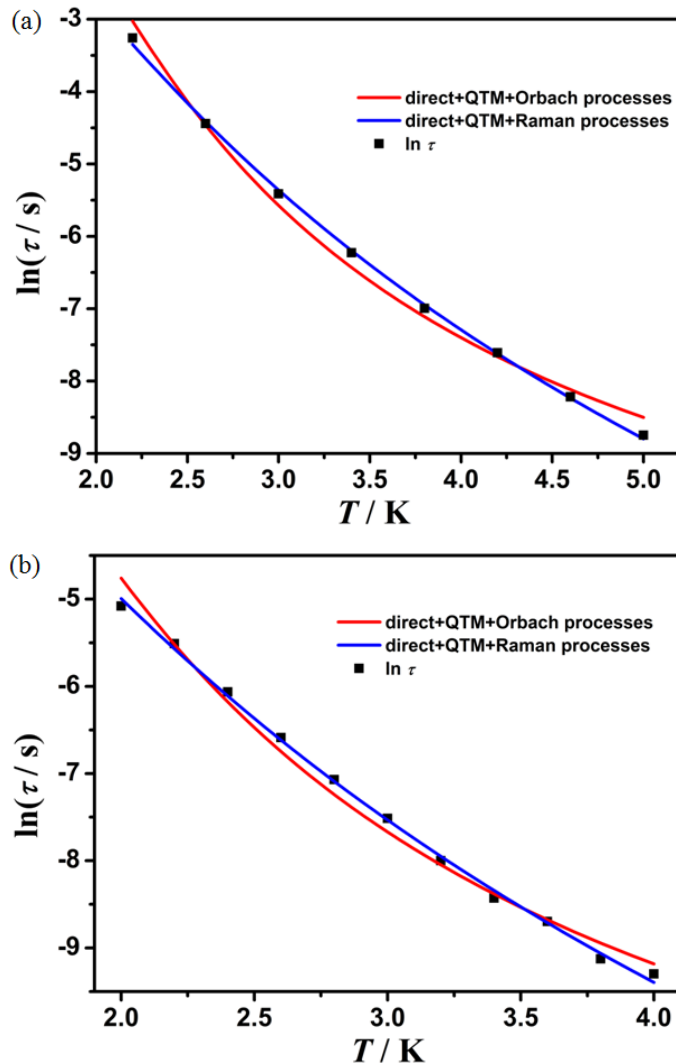


Fig.S8. The temperature-dependent relaxation time for **1** (a) and **2** (b) at 1.8K. The red lines are the fitness with direct, QTM and Orbach processes, while the blue lines are the fitness with direct, QTM and Raman processes.

Table S10. The fitting parameters of temperature-dependent relaxation data with the direct, QTM, Raman and Orbach processes for **1** (a) and **2** (b).*

	Processes	A ($s^{-1} Oe^{-4} K^{-1}$)	B_1 (s^{-1})	B_2 (Oe^{-2})	C ($s^{-1} K^n$)	n (s^{-1})	τ_0 (s)	U_{eff} (K)
1	direct+QTM+Raman	4.13E-15	11.29	1.50E-6	0.13	6.75	/	/
	direct+QTM+Orbach	4.13E-15	11.29	1.50E-6	/	/	2.48E-6	22
2	direct+QTM+Raman	1.08E-13	5330.37	1.36E-4	1.47	6.50	/	/
	direct+QTM+Orbach	1.08E-13	5330.37	1.36E-4	/	/	1.08E-6	18

*The parameters A , B_1 , B_2 are fixed in fitting field-dependent relaxation times, see Fig. S5and Table S8.

References:

1. J. Jankolovits, J. W. Kampf and V. L. Pecoraro, *Inorg. Chem.*, 2014, **53**, 7534.
2. G. M. Sheldrick, *Acta Crystallogr.*, 2008, **A64**, 112.
3. A. L. Spek, *Acta Crystallogr.*, 2015, **C71**, 9.
4. H. L. C. Feltham, R. Clérac, L. Ungur, V. Vieru, L. F. Chibotaru, A. K. Powell and S. Brooker, *Inorg. Chem.*, 2012, **51**, 10603-10612.
5. H. Yin, J. R. Robinson, P. J. Carroll, P. J. Walsh and E. J. Schelter, *Chem. Commun.*, 2014, **50**, 3470-3472.
6. T. Arliguie, L. Belkhiri, S.-E. Bouaoud, P. Thuéry, C. Villiers, A. Boucekkine and M. Ephritikhine, *Inorg. Chem.*, 2009, **48**, 221-230.
7. R. D. Rogers, A. N. Rollins, R. D. Etzenhouser, E. J. Voss and C. B. Bauer, *Inorg. Chem.*, 1993, **32**, 3451-3462.
8. R. K. Das, E. Barnea, T. Andrea, M. Kapon, N. Fridman, M. Botoshansky and M. S. Eisen, *Organometallics*, 2015, **34**, 742-752.
9. R. D. Rogers, A. N. Rollins, R. F. Henry, J. S. Murdoch, R. D. Etzenhouser, S. E. Huggins and L. Nunez, *Inorg. Chem.*, 1991, **30**, 4946-4954.
10. C. M. Zaleski, C.-S. Lim, A. D. Cutland-Van Noord, J. W. Kampf and V. L. Pecoraro, *Inorg. Chem.*, 2011, **50**, 7707-7717.
11. K. Gholivand, H. R. Mahzouni and M. D. Esrafil, *Dalton Trans.*, 2012, **41**, 1597-1608.
12. S. K. Gupta, T. Rajeshkumar, G. Rajaraman and R. Murugavel, *Chem. Commun.*, 2016, **52**, 7168-7171.
13. A. Bowden, S. J. Coles, M. B. Pitak and A. W. G. Platt, *Inorg. Chem.*, 2012, **51**, 4379-4389.
14. S. Pailloux, C. E. Shirima, E. N. Duesler, K. A. Smith and R. T. Paine, *Polyhedron*, 2011, **30**, 2746-2757.
15. A. W. Addison, T. N. Rao, J. Reedijk, J. van Rijn and G. C. Verschoor, *J. Chem. Soc., Dalton Trans.*, 1984, 1349-1356.
16. S. Hino, M. Maeda, K. Yamashita, Y. Kataoka, M. Nakano, T. Yamamura, H. Nojiri, M. Kofu, O. Yamamuro and T. Kajiwara, *Dalton Trans.*, 2013, **42**, 2683-2686.
17. S. Hino, M. Maeda, Y. Kataoka, M. Nakano, T. Yamamura and T. Kajiwara, *Chem. Lett.*, 2013, **42**, 1276-1278.
18. J. J. Le Roy, I. Korobkov, J. E. Kim, E. J. Schelter and M. Murugesu, *Dalton Trans.*, 2014, **43**, 2737-2740.
19. A. B. Khelifa, M. S. Belkhiria, G. Huang, S. Freslon, O. Guillou and K. Bernot, *Dalton Trans.*, 2015, **44**, 16458-16464.
20. C. Takehara, P. L. Then, Y. Kataoka, M. Nakano, T. Yamamura and T. Kajiwara, *Dalton Trans.*, 2015, **44**, 18276-18283.
21. J. D. Rinehart and J. R. Long, *Dalton Trans.*, 2012, **41**, 13572-13574.
22. A. Arauzo, A. Lazarescu, S. Shova, E. Bartolome, R. Cases, J. Luzon, J. Bartolome and C. Turta, *Dalton Trans.*, 2014, **43**, 12342-12356.
23. J. J. Baldoví, J. M. Clemente-Juan, E. Coronado, Y. Duan, A. Gaita-Ariño and C. Giménez-Saiz, *Inorg. Chem.*, 2014, **53**, 9976-9980.
24. J. J. Le Roy, S. I. Gorelsky, I. Korobkov and M. Murugesu, *Organometallics*, 2015, **34**, 1415-1418.